Energy materials

Synthetic tethered silver nanoparticles on reduced graphene oxide for alkaline oxygen reduction catalysis

Henry R. Tinker[1], Malavika A. Bhide[1], Emanuele Magliocca[2], Thomas S. Miller[2,*], and Caroline E. Knapp[1,*] (iD)

[1] *Department of Chemistry, University College London, 20 Gordon Street, London WC1H 0AJ, UK*
[2] *Electrochemical Innovation Lab, Department of Engineering, University College London, Torrington Place, London WC1E 7JE, UK*

ABSTRACT

There is currently an enormous drive to move away from the use of Pt group metals in catalysis, particularly for fuel cells, because of their increasing rarity and cost. Simultaneously, there have been advances in the application of graphene supported nanoparticular catalysts. However, these Pt-free, graphene supported catalysts can be complex to produce, show poor catalytic activity and degrade quickly due to particle agglomeration or isolation. Herein, we report a one-pot synthesis of silver nanoparticles (NPs) tethered to a reduced graphene oxide (rGO) template via organic linkages. This is one of the few silver precursor formations that have been combined with graphene oxide (GO) to simultaneously establish linkage binding sites, reduce GO and yield tethered nanoparticles. These materials are shown to efficiently catalyze the oxygen reduction reaction in alkaline environments, with aminoethanol linkages to 21.55 ± 2.88 nm Ag particles exhibiting the highest catalytic activity via the four-electron pathway. This method, therefore, offers a straightforward route to produce effective catalysts from inexpensive precursors, which could be developed further for significant industrial application.

GRAPHICAL ABSTRACT
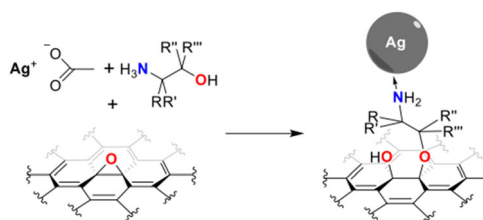
Introduction

New methods of materials synthesis are constantly being investigated in order to help face the progressive issues of clean energy generation and storage. Current major methods of energy generation still remain environmentally toxic and non-renewable, driving a greater demand for cleaner alternatives. Therefore, it is important to develop clean and efficient future energy generation technologies, as well as processes to synthesis the materials utilised. In this study, we aim to introduce a synthetic design that provides limited steps, via a 'one-pot' route, as well as a material that exhibits greater chemical activity and interaction through nanoparticular dative ligand tethering to a carbon-based template.

The aim of this synthesis is to provide an electrochemically stable and active material for methods of energy storage and so fully utilise these developing techniques of energy production [1, 2].

The ORR is a vital function for energy conversion in the functionality of metal air batteries and fuel cells. The main issue presenting itself is that platinum (Pt)-based catalysts still remain the most efficient and successful cathodes for these devices, for manufactured cells and the general market. This in turn stagnates the development of the production, forcing alternative sustainable research areas to be pursued. New and efficient non-Pt catalysts offer one route to overcome this barrier to industry.

Graphene oxide (GO) is a functionalised oxygenated variety of graphene, which is formed through the creation of oxygen defects upon the surface of graphite sheets via acidic functionalisation; this aids exfoliation [3]. The oxygen groups that reside on its surface are mainly composed of epoxy and hydroxyl groups, with a smaller abundance of carboxylic acids and ketones. These groups act as an active functionalisation site for a large variety of molecules to tether or react with, resulting in a multitude of applications for graphene oxide. Reduced graphene oxide (rGO), which results from chemical or thermal reduction of GO, has also attracted intensive research within this field, owing to its multitude of uses including energy storage, catalyst support or intrinsic catalysis [4, 5].

Anion exchange membrane fuel cells (AEMFCs) are a particularly favourable technology because, as opposed to their proton exchange counterparts, a number of 'non-precious' metal catalysts show high ORR activity in these alkaline conditions. Silver, which has very high electrical conductivity and ability to proceed via the 4-electron ORR pathway is particularly promising [6–8].

Whilst silver nitrate has been reported previously as a useful precursor for the functionalisation of rGO with silver nanoparticles (NPs), other methods of deposition, including chemical vapour deposition (CVD) and inkjet printing have employed a wider variety of silver precursors [9, 10]. Silver halides and inorganic silver salts, e.g. AgF and Ag(acetate), have been explored as precursors but again, high volatilisation and decomposition temperatures deem them unsuitable for low temperature studies [11]. The β-diketonate family of ligands has been used in silver precursors to deposit thin films, as their decomposition temperatures are low [12, 13]. Coyle et al. reported the deposition of silver films at the relatively low temperatures of 140–220 °C, using silver

iminopyrrolidinate precursors [14]. The synthesis of the precursor involved air sensitive techniques, creating a drawback for the isolation and industrial scalability of this precursor. Silver carboxylate precursors are also common, and the phosphane and phosphite adducts of silver carboxylate precursors have been widely researched, though requiring temperatures > 200 °C [15, 16]. CVD of silver films using triphenylphosphine and phenanthroline adducts of β-diketonates and β-diketoiminates was also reported, leading to metallic silver films being deposited at temperatures ranging from 200 to 550 °C. Successful depositions, however, yielded resistivity measurements more than ten times higher than that of bulk silver [17, 18].

Walker et al. reported the deposition of highly conductive metallic silver onto both glass and ethylene vinyl acetate at 90 °C in 15 min [19]. Consisting of silver acetate, ammonium hydroxide and formic acid, the reactive silver ink achieved conductivity equivalent to that of bulk silver. However, this formulation was prone to decomposition after a few weeks, and Vaseem et al. reported a modification of the formulation using 2-aminoethan-1-ol in place of ammonium hydroxide that gave their ink long-term stability [20]. Temperatures required to achieve metallic silver were higher than Walker et al.'s reports, and conductivities were lower than that of bulk silver. Further reports of modified formulations such as silver-ethylamine-ethanolamine-formate-complex and silver oxalate/ethylamine/ethyl alcohol/ethylene glycol which were both sintered at 150 °C on plastic substrates have also been reported [21, 22].

This study is the first to combine silver precursors with rGO synthetic methods to produce silver nanoparticles tethered to rGO sheets. Herein, we report the use of preformed silver amino-alcohol precursors that can be chemically bound to the epoxy functional groups simultaneously as GO is hydrothermally reduced. This research presents a facile alternative method to ORR performance, confirming that the ORR precedes preferentially via the four-electron route, producing water, as described herein.

Materials and methods

Materials

The chemicals used for this synthesis were purchased without purification. Graphite powder (< 20 micron), sulphuric acid (95%), hydrochloric acid (35%), phosphoric acid (> 85%), hydrogen peroxide (35.5%), potassium hydroxide pellets (puriss ≥ 86%), potassium permanganate (99%), Sodium Hydroxide 97%, 2-aminoethan-1-ol (≥ 99%), 1-aminopropan-2-ol (93%), 2-methyl-2-aminopropan-1-ol (≥ 99.0%), and silver nitrate (99%) were purchased from Sigma-Aldrich. Silver acetate (99%) was obtained from Alfa Aesar. Formic acid (99%) was from Fisher scientific.

Modified hummers method

Graphite powder (5 g) was vigorously mixed with phosphoric acid (H_3PO_4, 12.5 cm^3, 1 M) and sulphuric acid (H_2SO_4, 112.5 cm^3, 1 M) at a ratio of 1:9 at between 0 and 5 °C. Potassium permanganate ($KMnO_4$, 30 g) was slowly added, ensuring the temperature does not rise above 5 °C. This exothermic reaction produces a green/black mixture. The reaction was subsequently cooled back down to 0 °C and left to stir overnight. The mixture was allowed to reach room temperature for 3 h, before being very slowly heated to 50 °C in a silica oil bath, at increments of 5 °C maximum, to form a red product. Deionised water was slowly added to the mixture while constantly stirring, maintaining a temperature below 55 °C. Hydrogen peroxide (H_2O_2, 42.25 mL. 1 M) was added dropwise to remove any excess unreacted $KMnO_4$. This produced a bright yellow/orange mixture, which was left to stir at 50 °C for 1 h, before being left unstirred overnight, in order to remove any excess water. This resulted in a light brown GO mixture being formed. This product was subsequently washed with hydrochloric acid (HCl, 2 cm^3, 0.1 M) and centrifuged to remove any remaining unwanted salts. The GO was washed further with deionised water until pH was between 5.5 and 7. This was dried under vacuum for 3 days until the product was dry.

The GO powder was dispersed in deionised water (2 mg cm^{-3}) and ultra-sonicated using a sonicating probe to ensure optimal particle dispersion for 6–8 h. The dispersed GO was hydrothermally reduced via the use of an autoclave at 180 °C for 12 h to form

rGO. The product was filtered and dried using a vacuum oven at 60 °C overnight. To increase porosity, the material was freeze dried under vacuum for 3 days, depending on quantity.

Reduced graphene oxide—silver nitrate

GO (100 mg), silver nitrate (2.6 mM) and DI water (400 mL) were ultrasonicated under a nitrogen flow for 2 h. Sodium hydroxide (44 mL, 8 M) was slowly added, while the mixture was being stirred at 80 °C for 20 h. The resultant mixture was centrifuged (5500 rpm) for 15 min lengths, 3–4 times to remove any unreacted NaOH with DI water.

Silver precursor synthesis

Silver acetate ($AgC_2H_3O_2$, 1.0017 g, 6 mmol) was added to ammonium hydroxide (NH_4OH, 2.5 cm^3, 20 mmol) and was stirred under ambient conditions for 15 min. Under sonication, formic acid (CH_2O_2, 0.2 cm^3, 5 mmol) was added dropwise to ensure thorough distribution, with the solution being further mixed with use of a vortex. Any silver metal particles that form in the solution are produced because of the reduction of silver ions via the formic acid. The solution was filtered and stored in a dark place to ensure degradation of the silver precursor ($Ag(OCHO).x(NH_3)_2$).

Silver acetate ($AgC_2H_3O_2$, 2.0063 g, 12 mmol) was added to 2-aminoethan-1-ol ($CH_3CH(NH_2)OH$, 4 cm^3, 4.04 g, 66 mmol) and deionised water (4 cm^3) and was stirred under ambient conditions for 15 min. Under sonication, formic acid (CH_2O_2, 0.2 cm^3, 5 mmol) was added dropwise to ensure thorough distribution, with the solution being further mixed with use of a vortex forming the silver precursor ($Ag(OCHO).x$ ($CH_3CH(NH_2)OH)_2$).

Silver acetate ($AgC_2H_3O_2$, 2.0049 g, 12 mmol) was added to 1-aminopropan-2-ol ($CH_3CH(OH)CH_2NH_2$, 4 cm^3, 3.89 g, 52 mmol) and deionised water (4 cm^3) and was stirred under ambient conditions for 15 min. Under sonication, formic acid (CH_2O_2, 0.2 cm^3, 5 mmol) was added dropwise to ensure thorough distribution, with the solution being further mixed with use of a vortex forming the silver precursor ($Ag(OCHO).x$ (($CH_3CH(OH)CH_2NH_2)_2$).

Silver acetate ($AgC_2H_3O_2$, 1.0099 g, 6 mmol) was added to 2-methyl-2-aminopropan-1-ol (($CH_3)_2$ $C(NH_2)CH_2OH$, 2 cm^3, 1.87 g, 21 mmol) and

deionised water (4 cm^3) and was stirred under ambient conditions for 15 min. Under sonication, formic acid (CH_2O_2, 0.2 cm^3, 5 mmol) was added dropwise to ensure thorough distribution, with the solution being further mixed with use of a vortex forming the silver precursor ($Ag(OCHO).x$ (($CH_3)_2$ $C(NH_2)CH_2OH)_2$).

All of the precursors will form silver metal particles when formic acid is added, which requires separation via filtration. All need to be stored in the dark to prevent silver degradation.

Silver precursor + rGO

GO (100 mg) was added to deionised water (10 cm^3) and sonicated for 1.5 h to ensure thorough dispersion. The silver precursor (25 μm^3, 50 μm^3, 100 μm^3, 200 μm^3) was added dropwise to the solution and was further sonicated for 2 h. The mixture was placed in an autoclave and was heated to 180 °C for 12 h, before being filtered, washed and freeze dried under vacuum.

Electrochemical measurements

Electrochemical tests were carried out in a three-electrode system using a potentiostat (Gamry Interface 1000E). A glassy carbon (GC) electrode (diameter of 5 mm with surface area of 0.196 cm^2) was used as a working electrode, with a platinum grid counter electrode and a Ag/AgCl (saturated KCl) reference electrode. To prepare the working electrode, typically, 10 mg of catalyst with 30 μL of Nafion solution (Nafion^{TM} D521, 5 wt% dispersion) was dispersed in 2 mL of H_2O:IPA (1:1) by sonicating for 1 h to form a homogeneous ink. Then 9 μL of the dispersion was loaded onto a electrode (loading 100 μg cm^{-2}) through drop casting, and the electrode was dried. Before ORR catalytic activity testing, oxygen bubbled through a 0.1 M KOH solution for 30 min to enure solution oxygen saturation. The working electrodes were also activated using cyclic voltammetry, by scanning them at a scan rate of 100 mV s^{-1} between − 0.9 and 0.6 V vs. Ag/AgCl in the O_2 saturated 0.1 M KOH for 100 cycles. Linear sweep voltammetry (LSV) was then used to test the ORR activity at a scan rate of 20 mV s^{-1}, again in O_2-saturated 0.1 M KOH. Polarization curves (i.e. LSVs) were measured from − 0.7 to 0.1 V (vs. Ag/AgCl) at

rotation speeds between 400 and 2500 rpm, controlled using a MSR Electrode Rotator (Pine Research Instrumentation. A commercial Ag/C catalyst (PK Catalyst, 40% Silver supported on Vulcan XC-7240) was used as the reference material with the same loading. Koutecky–Levich plots (j^{-1} vs $\omega^{-1/2}$) were analysed at various electrode potentials. The slope of their linear fit was used to calculate the electron transfer number (n) based on the Koutecky–Levich equation:

$$j^{-1} = j_K^{-1} + j_L^{-1} = j_K^{-1} + \left(B\omega^{1/2}\right)^{-1} \quad (1)$$

where j is the measured current density, j_K is the kinetic current density of the ORR, and ω is the angular velocity of rotation. Here, B is related to the diffusion-limited current density through the expression $j_L = B\omega^{1/2}$, which can be defined as:

$$B = 0.62nFC_O(D_O)^{2/3}\nu^{-1/6} \quad (2)$$

where n is the overall number of electrons transferred during the oxygen reduction, F is the Faraday constant (96485 C mol^{-1}), ν is the kinematic viscosity of the solution (0.01 cm^2 s^{-1}), D_O is the diffusion coefficient of oxygen (1.9 × 10^{-5} cm^2 s^{-1}), and C_O is the concentration of oxygen in the bulk (1.2 × 10^{-6} mol cm^{-3}) [23, 24].

Instruments

The samples underwent a series of characterisation procedures in order to study their morphology and design. This was performed with scanning electron microscopy (SEM, Jeol 6700) and transmission electron microscopy (TEM, Jeol 2100), X-ray photoemission (XPS) results were measured and obtained by Al-K-α, Thermo Scientific. The FT-IR was obtained with the ALPHA FTIR routine spectrometer. Raman spectra were recorded using a 514.5 nm laser beam (Renishaw).

Results and discussion

To establish a strong point of comparison we began with replicating the work of Tian et al. combining silver nitrate and GO under chemical reduction conditions, yielding **A**—a mixture of silver NPs on rGO [25]. Consistent with the literature, XPS (Fig. 1a) and TEM images (Fig. 2a) show the reduction of GO and
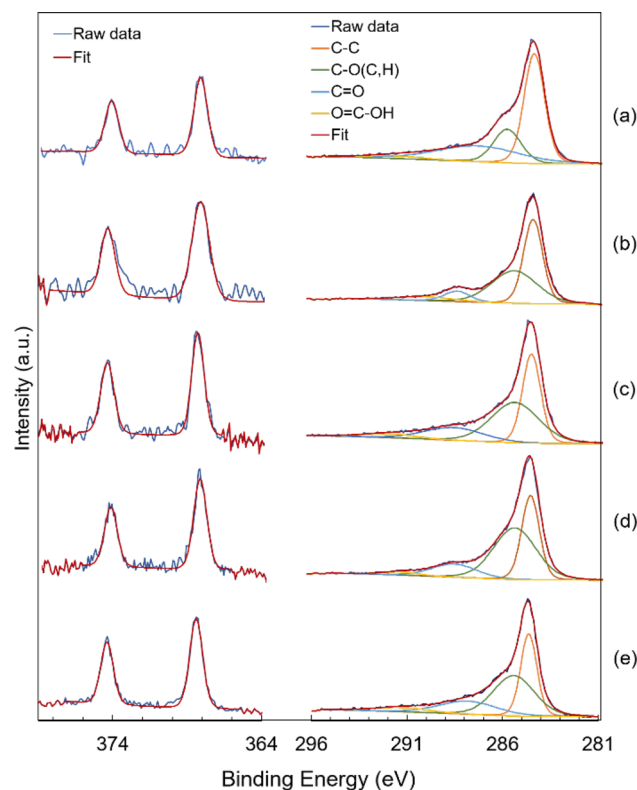

Figure 1 XPS data showing the Ag 3d, and C 1 s of different variations of Ag NP-rGO composites: samples **A** to **E**.

its silver NPs sized below 20 nm. In a view to remove NaOH from the synthesis, a corrosive and harmful reagent, a second route to Ag NPs on rGO was employed. In this experiment, the silver precursor formulation first reported by Walker et al. was added to GO, this time using a hydrothermal aqueous route, removing the need for sodium hydroxide entirely— yielding **B**. Interestingly both samples **A** and **B** show similar Raman spectra (Fig. 3a), illustrating how neither method of deposition alters the bonding interaction on the surface of rGO, however, TEM images of **B** reveal the Ag NPs to be sparse, as described in more detail later. The ICP-MS of sample **B** also reveals the percentage of Ag to be within a similar range to the other composites, within a 14–31% weight (SI Table S3) loading, but due to this precursor formulation being prone to decomposition, it is therefore less effective for functionalising rGO sheets [10, 26].

To illustrate our approach, a combination of silver acetate, formic acid and a range of amino-alcohols of the type HOCRR'CR''R'''NH$_2$ (R, R', R'', R''' = H (**AE**); R, R'', R''' = H, R' = Me (**AP**); R, R' = H, R'',
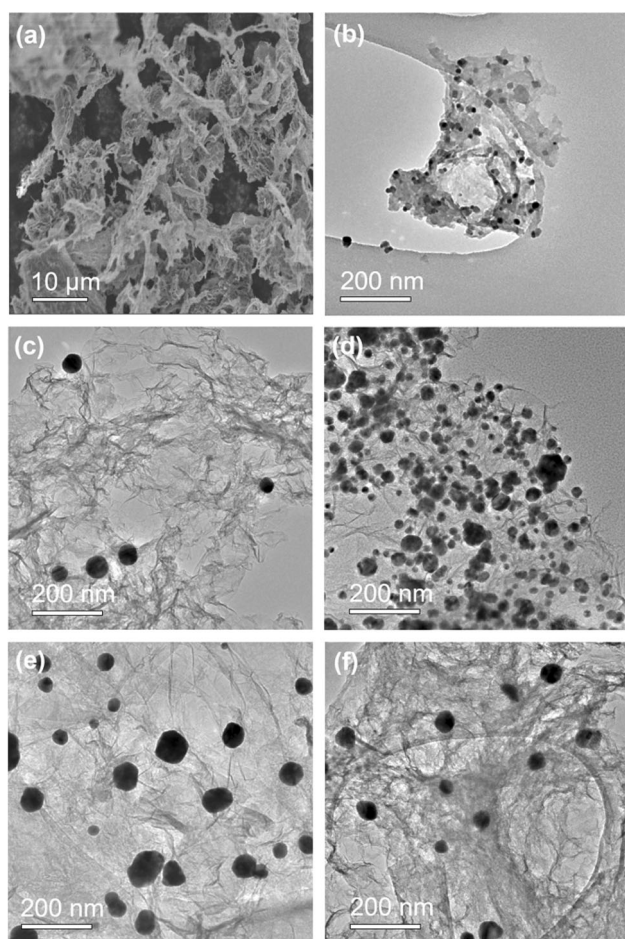
Figure 2 a representative SEM image of a Ag NP rGO composite, in this case from sample **C** (remainder in SI), **b–f** TEM images of Ag NP rGO composites from samples **A** to **E**, respectively.
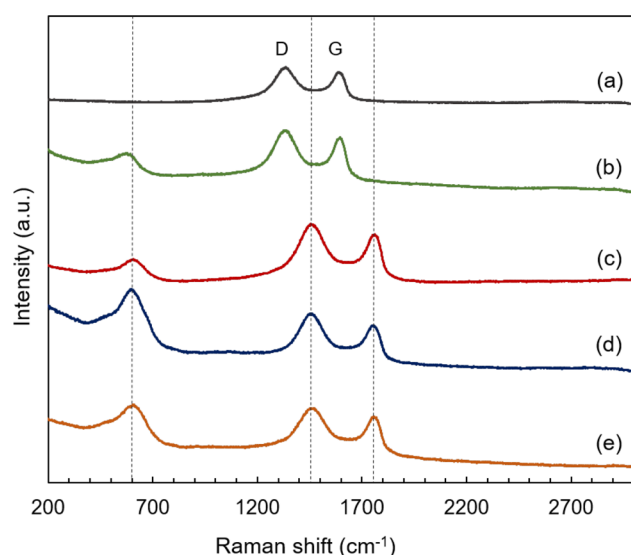

Figure 3 Raman spectra of samples **A** to **E**.

R''' = Me (**AMP**)), which would act as tethering agents, were combined with GO in hydrothermal syntheses to produce Ag·NP bound to rGO sheets. The simple amino-alcohol **AE** produced sample **C**, addition of a methyl group to the chain in **AP** yielded **D** and the bulkier **AMP** gave sample **E** (see Scheme 1).

To understand how the precursors bind to the surface of the rGO, it is important to acknowledge the various mechanisms of surface oxidation during the synthesis of GO [27]. Most of the oxide groups form via the surface oxidation of graphite with use of manganite ions. The ion attacks a bond positioned next to acetone to form a carboxylic acid, before forming the epoxy group via a leaving alcohol group (SI Figure S1). Hydrothermal reduction was used to remove or alter surface oxygen functional groups. In the case of the epoxy group it undergoes a regioselective S_N2 reaction [28]. The hydroxide will target the electrophile in a less hindered position once the epoxy oxygen has been protonated, forming another alcohol group.

Employing this model, we propose that the OH group on each amino-alcohol in **C**, **D** and **E**, respectively, undergoes this S_N2 mechanism to bind to the less sterically hindered/less substituted carbon. The amine end remains datively interacted with the Ag NP which has formed in situ from reaction of the silver acetate precursor with the formic acid additive, thus preventing a high level of aggregation. The precursor formulations used in the synthesis of **C**, **D** and **E** have each yielded Ag NP tethered to rGO sheets, as evidenced by the Raman spectra (Fig. 3).

Observing the XPS of samples **A** to **E** reveals the degree to which the oxygen functional groups on the carbon are reduced and if the different precursors have any influence over the level or type of reduction. It can be seen in the XPS of samples **A** to **E** (Fig. 1) that only a metallic silver environment is observed. For all samples Ag 3d peaks at 368 ± 0.2 eV and 374 ± 0.2 eV corresponding to the Ag $3d_{5/2}$ and $3d_{3/2}$, respectively, consistent with literature values for silver (368.2 eV ($3d_{5/2}$) and 374.2 ($3d_{3/2}$)) [29]. By observing the carbon environments in the second column for samples **A** to **E** we can note the level of reduction the GO has undergone, specifically observing which oxygen functional groups have been targeted. The C 1 s peaks generally show the same level of reduction throughout apart from with sample
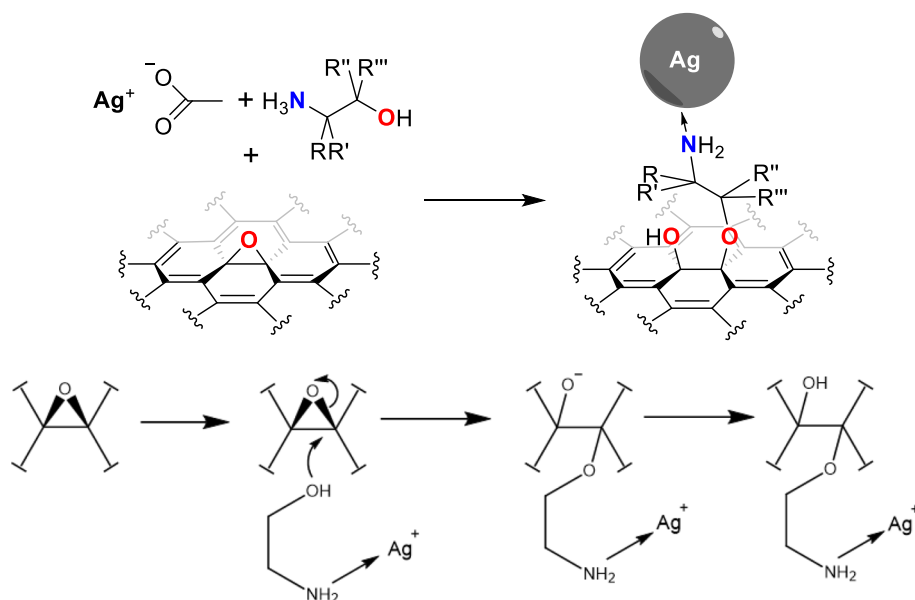
A, where it is likely that the NaOH may have played a role in reducing the C=O group.

The effect of using different silver precursor formulations on the synthesis of rGO from GO is revealed in the TEM images. The faithful reproduction of Tian et al.'s Ag NP rGO composites (sample **A**) reveal a more densely layered reduced graphene oxide, indicating thicker layers and a reduced surface area [25]. The remaining samples **B–E** have each been synthesised using an aqueous hydrothermal route and as such the TEM images indicate very thin layers, shown by their wrinkling and almost transparent imaging. This provides a better surface interaction with the Ag NPs which is clearly reflected in the ORR catalysis results reported below. It can be noted the variation in size and dispersion of the silver particles across the carbon surface varies dependent on synthetic route. Tian et al.'s NaOH method to sample **A** produced the smallest particle size, varying between 19.17 ± 2.88 nm in size (SI Table S1). This was followed sample **C** which used the simplest amino-alcohol (**C**) as a tethering agent, producing slightly larger particles (21.55 ± 2.88 nm) with particles exhibiting excellent dispersion across the surface of the rGO. The TEM images of **B**, **D** and **E** show particles with sizes between 60 and 120 nm, with only moderate dispersion. This is potentially attributed to the size and dexterity of the larger precursor ligand and its laboured interactions with the surface epoxy groups, causing it to clump and form silver metal.

Raman spectra are important in defining the nature and interactions of the silver precursors with reduced graphene oxide. It can be noted that two major peaks that define the rGO are represented by lower shifted D band (~ 1350 cm^{-1}), illustrating the graphene oxide's disordered sp^2 carbon structure and the G band (~ 1500 cm^{-1}) that indicated C–C stretching. In samples **C**, **D** and **E**, (i.e. the Ag NP rGO composites formed using amino-alcohols to tether the NP to the rGO) there is a noticeable shift in the D and G bands by around 10 cm^{-1}. This shift can be potentially be attributed to the change in C–C bond lengths on the surface of the rGO from the external influence of the precursors. The peaks assigned to with the smaller Raman shift, around 500–700 cm^{-1}, are likely to be the N–C–O, that are not found in conventional rGO and distinguishes the data.

To evaluate the performance of the as-prepared Ag NP rGO composites for oxygen reduction electrocatalysis rotating disk electrode (RDE) experiments were performed in an O$_2$-saturated 0.1 M KOH solution (Fig. 4). Using a 5 mm GC RDE, modified with the as-synthesised Ag catalysts or a commercial Ag/C (see methods), LSVs were measured at a rotation speed of 1600 rpm (Fig. 4a). These showed that tethered Ag catalysts **C**, **D** and **E** offer a notably more positive (i.e. lower overpotential) onset potential, compared with the commercial Ag/C (**Ag/C**). In particular, the onset potential for **C** (0.01 V vs. Ag/AgCl) is close to 70 mV more positive, with a similar overall current density, than Ag/C, indicating
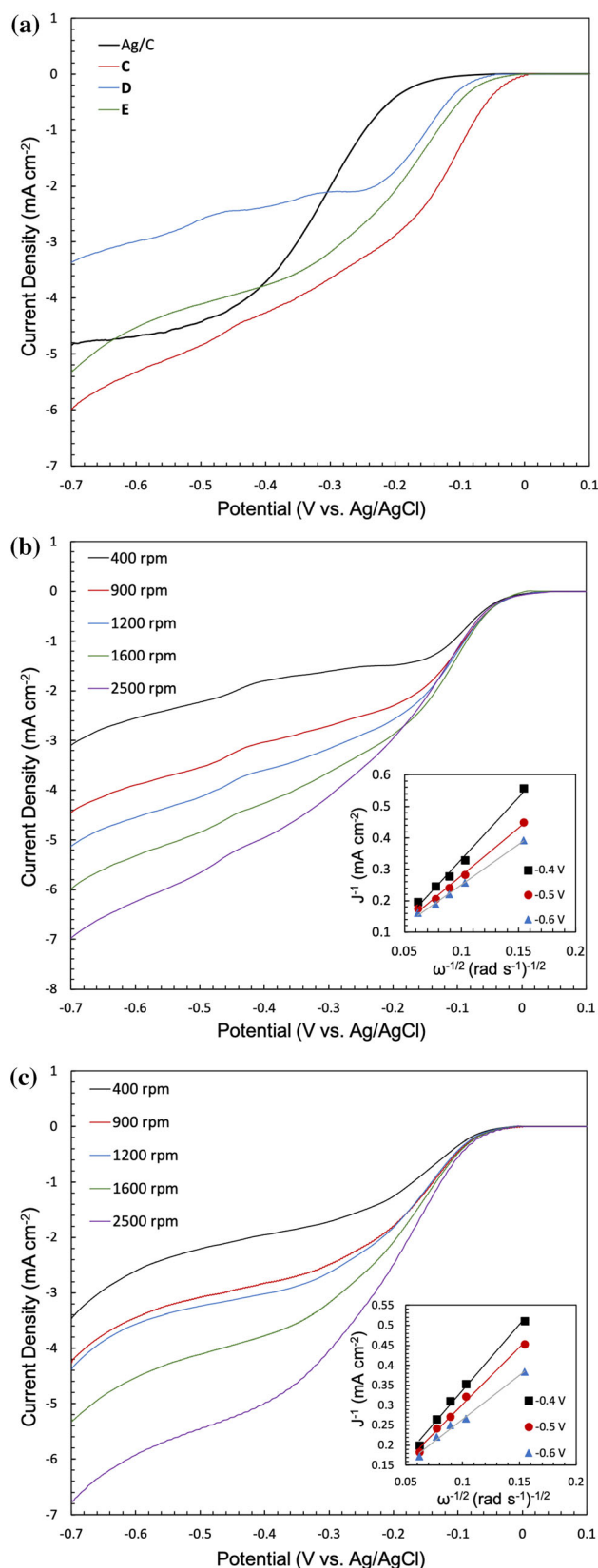
◄ **Figure 4** ORR at Ag catalysts: **a** LSVs of **C**, **D** and **E** tethered Ag particles, alongside a commercial Ag/C catalyst at 1600 rpm. **b**, **c** Rotation rate dependent LSVs and inset Koutecky–Levich plots for **C**; **b** and **D**; **c**, respectively. All recorded in an O_2-saturated 0.1 M KOH solution at a scan rate of 20 mV s^{-1}.

notably improved catalytic activity. This compares favourably with literature values for novel Ag ORR electrocatalysts and commercial Pt/C under similar conditions (see supporting information, Fig. S8) [7, 30, 31]. Sample **E** also produces a similar current density to the **Ag/C**, although with a less positive onset potential than **C**, whereas sample **D** shows a notably lower current density, almost half that of the other catalysts. This may suggest sample **D** (**AP** precursor) is only undertaking a partial ORR to produce H_2O_2.

Rotation rate dependent LSV curves for **C** and **E** catalysts, recorded from 400 to 2500 rpm, are shown in Fig. 4b and c, respectively. From these, Koutecky–Levich (K–L) plots were obtained (j^{-1} vs $\omega^{-1/2}$—see methodology for details). As the LSVs did not reach a clear plateau, attributed to increasing background catalytic contributions from the rGO, the rotation rate dependant current at three potentials close the apparent limiting value were used (− 0.4, − 0.5 and − 0.6 V vs. Ag/AgCl) [32]. The K–L plots at all chosen potentials exhibited good linearity, and thus, the electron transfer number could be extracted from the slope according to the K–L equation. Here the number of electrons transferred per oxygen molecule was found to be n = 3.0, 3.5 and 4.0 at − 0.4, − 0.5 and − 0.6 V vs. Ag/AgCl, respectively, for **C**, whereas n = 3.1, 3.5 and 4.1 at the same voltages for **E**. All values are close to four, confirming that the ORR was proceeding via the four-electron, or pseudo-four-electron (via H_2O_2), route, producing water (Figure S9) [7]. The Y-intercept of the K-L plot is close zero, indicating fast electron transfer kinetics [24]. Comparison with the experimentally observed rotation rate dependent limiting current with calculated theoretical values further indicate a four-electron ORR (see supporting information).

Samples D and E exhibit similar Ag particle size, but it is interesting to observe how the ORR activities are different. The variation of onset potential from linker to linker is likely an effect of the relative pKa values of the respective amino-alcohols effecting their

binding abilities (pKa: AE = 9.5, AP = 15.3 AMP = 9.7). The linker in sample D is the most basic and such it follows that the onset potential is the highest of the three. It is well known that surface functionalisation of rGO, particularly with bound N species will alter onset potential, as is evidenced in the data reported here (Fig. 4) [33]. These data confirm that the tethering via aminoethanol linkages influences the Ag catalysts. This may be due to a direct effect of the functional linkage on the metal, via electron withdrawing for examole or due to increased particle stability. When combined with the one pot nature of the synthetic procedure, this therefore suggests this methodology has great potential for the creation of practical and effecient future catalysts at scale.

Conclusion

We have shown, for the first time, that the combination of novel silver precursor formulations (including a range of amino-alcohol ligands) with GO in a hydrothermal synthesis has produced Ag NP bound to rGO sheets. The route employing the simple amino-alcohol **AE** (sample **C**), shows the most distributed and even particle size (12–25 nm). All three amino-alcohol incorporated samples (**C**–**E**) reveal shifts in their Raman spectra, consistent with tethering of the amino-alcohol to the rGO surface which is not present in samples **A** and **B**. Samples **A** and **B**, which have been included in this work for a point of comparison do not use amino-alcohols in their synthesis, and as such the Ag NP are not tethered. This work represents a simple, scalable, non-toxic (aqueous hydrothermal) route to produce functional Ag NP rGO composites with high catalytic performance for the ORR. Therefore, this synthesis has great potential as a route to produce inexpensive, high performance catalysts for future AEM fuel cells and beyond.

Acknowledgements

Compliance with ethical standards

Conflict of interest   The authors declare no conflict of interest.

Supplementary Information: The online version of this article (https://doi.org/10.1007/s10853-020-057 11-2) contains supplementary material, which is available to authorized users.

Supplementary Information: The online version of this article (https://doi.org/10.1007/s10853-020-057 11-2) contains supplementary material, which is available to authorized users.

References

[1]   Ould Amrouche S, Rekioua D, Rekioua T, Bacha S (2016) Overview of energy storage in renewable energy systems. Int J Hydrog Energy 41(45):20914–20927. https://doi.org/10.1016/j.ijhydene.2016.06.243

[2]   Olabi AG (2017) Renewable energy and energy storage systems. Energy 136:1–6. https://doi.org/10.1016/j.energy.2017.07.054

[3]   Dreyer DR, Park S, Bielawski CW, Ruoff RS (2010) The chemistry of graphene oxide. Chem Soc Rev 39(1):228–240. https://doi.org/10.1039/b917103g

[4]   Chabot V, Higgins D, Yu A, Xiao X, Chen Z, Zhang J (2014) A review of graphene and graphene oxide sponge: material synthesis and applications to energy and the environment.

Energy Environ Sci 7(5):1564–1596. https://doi.org/10.1039/c3ee43385d

[5] Wang S, Li F, Wang Y, Qiao D, Sun C, Liu J (2018) A superior oxygen reduction reaction electrocatalyst based on reduced graphene oxide and iron (II) phthalocyanine-supported sub-2 Nm platinum nanoparticles. ACS Appl Nano Mater 1(2):711–721. https://doi.org/10.1021/acsanm.7b00173

[6] Naghdi S, Rhee KY, Hui D, Park SJ (2018) A review of conductive metal nanomaterials as conductive transparent and flexible coatings thin films and conductive fillers: different deposition methods and applications. Coatings. https://doi.org/10.3390/coatings8080278

[7] Erikson H, Sarapuu A, Tammeveski K (2019) Oxygen reduction reaction on silver catalysts in alkaline media: a minireview. ChemElectroChem 6(1):73–86. https://doi.org/10.1002/celc.201800913

[8] Sun C, Alonso JA, Bian J (2020) Recent advances in perovskite-type oxides for energy conversion and storage applications. Adv Energy Mater. https://doi.org/10.1002/aenm.202000459

[9] Kumar S, Mahajan M, Singh R, Mahajan A (2018) Silver nanoparticles anchored reduced graphene oxide for enhanced electrocatalytic activity towards methanol oxidation. Chem Phys Lett 693:23–27. https://doi.org/10.1016/j.cplett.2018.01.003

[10] Knapp CE, Chemin JB, Douglas SP, Ondo DA, Guillot J, Choquet P, Boscher ND (2018) Room-temperature plasma-assisted inkjet printing of highly conductive silver on paper. Adv Mater Technol 3(3):1–6. https://doi.org/10.1002/admt.201700326

[11] Voorhoeve RJH, Merewether JW (1972) Selective deposition of silver on silicon by reaction with silver fluoride vapor. J Electrochem Soc 119(3):364. https://doi.org/10.1149/1.2404203

[12] Partenheimer W, Johnson EH (1973) Heats of reaction of triphenylphosphine with compounds of the type hexafluoroacetylacetonato (Olefin) silver (I). Inorg Chem 12(6):1274–1278. https://doi.org/10.1021/ic50124a012

[13] Politova ED, Kaleva GM, Furaleva KI, Prutchenko SG (1998) The microstructure and superconducting properties of YBa$_2$ Cu$_3$ Oy—based ceramics. Jpn J Appl Phys 7(L1504):73–80. https://doi.org/10.1002/9781118407165.ch10

[14] Coyle JP, Gordon PG, Wells AP, Mandia DJ, Sirianni ER, Yap GPA, Barry ST (2013) Thermally robust gold and silver iminopyrrolidinates for chemical vapor deposition of metal films. Chem Mater 25(22):4566–4573. https://doi.org/10.1021/cm402658c

[15] Szłyk E, Piszczek P, Grodzicki A, Chaberski M, Goliński A, Szatkowski J, Błaszczyk T (2001) CVD of AgI complexes with tertiary phosphines and perfluorinated carboxylates—a new class of silver precursors. Chem Vap Depos 7(3):111–116. https://doi.org/10.1002/1521-3862(200105)7:3%3c111::AID-CVDE111%3e3.0.CO;2-V

[16] Jakob A, Schmidt H, Djiele P, Shen Y, Lang H (2006) Phosphane/phosphite silver(I) carboxylates as CVD precursors. Microchim Acta 156(1–2):77–81. https://doi.org/10.1007/s00604-006-0592-z

[17] Edwards DA, Mahon MF, Molloy KC, Ogrodnik V (2003) Aerosol-assisted chemical vapour deposition of silver films from adducts of functionalised silver carboxylates. J Mater Chem 13(3):563–570. https://doi.org/10.1039/b210085c

[18] Liu H, Battiato S, Pellegrino AL, Paoli P, Rossi P, Jiménez C, Malandrino G, Muñoz-Rojas D (2017) Deposition of metallic silver coatings by aerosol assisted MOCVD using two new silver β-diketonate adduct metalorganic precursors. Dalt Trans 46(33):10986–10995. https://doi.org/10.1039/c7dt01647f

[19] Walker SB, Lewis JA (2012) Reactive silver inks for patterning high-conductivity features at mild temperatures. J Am Chem Soc 134(3):1419–1421. https://doi.org/10.1021/ja209267c

[20] Vaseem M, Lee SK, Kim JG, Hahn YB (2016) Silver-ethanolamine-formate complex based transparent and stable ink: electrical assessment with microwave plasma vs thermal sintering. Chem Eng J 306:796–805. https://doi.org/10.1016/j.cej.2016.08.003

[21] Vaseem M, McKerricher G, Shamim A (2016) Robust design of a particle-free silver-organo-complex ink with high conductivity and inkjet stability for flexible electronics. ACS Appl Mater Interfaces 8(1):177–186. https://doi.org/10.1021/acsami.5b08125

[22] Dong Y, Li X, Liu S, Zhu Q, Li JG, Sun X (2015) Facile synthesis of high silver content MOD ink by using silver oxalate precursor for inkjet printing applications. Thin Solid Films 589:381–387. https://doi.org/10.1016/j.tsf.2015.06.001

[23] Vikkisk M, Kruusenberg I, Joost U, Shulga E, Tammeveski K (2013) Electrocatalysis of oxygen reduction on nitrogen-containing multi-walled carbon nanotube modified glassy carbon electrodes. Electrochim Acta 87:709–716. https://doi.org/10.1016/j.electacta.2012.09.071

[24] Bard AJ, Faulkner LR (2001) Electrochemical Methods: Fundamentals and Applications, 2nd edn. Elsevier, Amsterdam

[25] Tian J, Liu S, Zhang Y, Li H, Wang L, Luo Y, Asiri AM, Al-Youbi AO, Sun X (2012) Environmentally friendly, one-pot synthesis of ag nanoparticle-decorated reduced graphene

oxide composites and their application to photocurrent generation. Inorg Chem 51(8):4742–4746. https://doi.org/10.1021/ic300332x

[26] Vaseem M, Lee S-K, Kim J-G, Hahn Y-B (2016) Silver-ethanolamine-formate complex based transparent and stable ink—electrical assessment with microwave plasma vs thermal sintering—elsevier enhanced reader. Pdf. Chem Eng J 306(1385–8947):796–805

[27] Compton OC, Nguyen ST (2010) Graphene oxide, highly reduced graphene oxide, and graphene: versatile building blocks for carbon-based materials. Small 6(6):711–723. https://doi.org/10.1002/smll.200901934

[28] Kang JH, Kim T, Choi J, Park J, Kim YS, Chang MS, Jung H, Park KT, Yang SJ, Park CR (2016) Hidden second oxidation step of hummers method. Chem Mater 28(3):756–764. https://doi.org/10.1021/acs.chemmater.5b03700

[29] Hoflund GB, Hazos ZF, Salaita GN (2000) Surface characterization study of Ag, AgO, and Ag_2O using x-ray photoelectron spectroscopy and electron energy-loss spectroscopy. Phys Rev B Condens Matter Mater Phys 62(16):11126–11133. https://doi.org/10.1103/PhysRevB.62.11126

[30] Ji D, Wang Y, Chen S, Zhang Y, Li L, Ding W, Wei Z (2018) Nitrogen-doped graphene wrapped around silver nanowires for enhanced catalysis in oxygen reduction reaction. J Solid State Electrochem 22(7):2287–2296. https://doi.org/10.1007/s10008-018-3914-2

[31] Soo LT, Loh KS, Mohamad AB, Daud WRW, Wong WY (2016) Synthesis of silver/nitrogen-doped reduced graphene oxide through a one-step thermal solid-state reaction for oxygen reduction in an alkaline medium. J Power Sourc 324:412–420. https://doi.org/10.1016/j.jpowsour.2016.05.106

[32] Bikkarolla SK, Cumpson P, Joseph P, Papakonstantinou P (2014) Oxygen Reduction reaction by electrochemically reduced graphene oxide. Faraday Discuss 173:415–428. https://doi.org/10.1039/c4fd00088a

[33] Sherbow TJ, Fettinger JC, Berben LA (2017) Control of ligand PKa values tunes the electrocatalytic dihydrogen evolution mechanism in a redox-active aluminum (III) complex. Inorg Chem 56(15):8651–8660. https://doi.org/10.1021/acs.inorgchem.7b00230